

Reversal of chloride-induced Cu(001) subsurface buckling in the electrochemical environment: An *in situ* surface x-ray diffraction and density functional theory study

Y. Gründer, D. Kaminski,* F. Golks, K. Krug, J. Stettner, and O. M. Magnussen
Institut für Experimentelle und Angewandte Physik, Universität Kiel, Olshausenstr. 40, 24098 Kiel, Germany

A. Franke, J. Stremme, and E. Pehlke
Institut für Theoretische Physik und Astrophysik, Universität Kiel, Olshausenstr. 40, 24098 Kiel, Germany
 (Received 20 October 2009; published 20 May 2010)

The interface of Cu(001) electrode surfaces in 10 mM HCl solution was studied by *in situ* surface x-ray diffraction and density functional theory, focusing on the precise structure of the $c(2 \times 2)$ Cl adlayer formed at positive potentials. Crystal truncation rod measurements in this adsorbate phase at a potential of $-0.20 \text{ V}_{\text{Ag}/\text{AgCl}}$ reveal distinct differences to corresponding data by Tolentino *et al.* [Surf. Sci. **601**, 2962 (2007)] for the $c(2 \times 2)$ Cl structure formed at the Cu(001)-vacuum interface. Although in both environments, the atoms in the second Cu layer exhibit a small vertical corrugation, the sign of this corrugation is reversed. Furthermore, also the Cu-Cl bond distance and the average Cu interlayer spacings at the surface differ. *Ab initio* calculations performed for this adsorbate system reproduce these effects—specifically the reversal of the subsurface second-layer buckling caused in the presence of coadsorbed water molecules and cations in the outer part of the electrochemical double layer. In addition, studies at more negative potentials reveal a continuous surface phase transition to a disordered Cl adlayer at $-0.62 \text{ V}_{\text{Ag}/\text{AgCl}}$, but indicate a substantial Cl coverage even at the onset of hydrogen evolution.

DOI: [10.1103/PhysRevB.81.174114](https://doi.org/10.1103/PhysRevB.81.174114)

PACS number(s): 61.05.cf, 68.08.-p, 68.43.-h, 71.15.Mb

I. INTRODUCTION

The atomic-scale structure of the metal-electrolyte interface is a topic of central importance to interfacial electrochemistry and has been studied extensively by electrochemical measurements, structure-sensitive *in situ* techniques, as well as by theoretical methods. In particular, adsorbate layers of strongly chemically bound (“specifically adsorbed”) anions, such as halide or sulfate, have been investigated in great detail, revealing a complex, potential-dependent two-dimensional (2D) phase behavior, which can significantly affect electrochemical reactions such as galvanic deposition, etching, corrosion, and electrocatalytic processes.¹ Often very similar superstructures are observed as those found in studies under ultrahigh vacuum (UHV) conditions after adsorption of the corresponding gaseous species from the gas phase. Nevertheless, complete structural agreement is not expected since in electrochemical environment the presence of physisorbed species in the so-called diffuse double layer—notably coadsorbed water and cations—leads to pronounced changes in the electrostatic potential drop at the interface, as revealed by UHV model studies on simulated double layers.^{2,3} The precise influence of these effects on the interface structure is still unclear. Specifically, up to now only a few studies have presented detailed measurements of the bond lengths at electrochemical interfaces that could be directly compared to structural data on corresponding anionic adlayer structures under UHV conditions.^{4–9} Such comparative studies allow to clarify how the presence of the outer part of the double layer alters the chemical bonding of the chemisorbed inner adsorbate layer to the surface and the near surface structure of the metal electrode, which in turn may throw light on the interplay among the interactions of the various species at the interface, the charge distribution, and

the interface structure. Here we present a combined surface x-ray diffraction (SXR) and density-functional theory (DFT) study of Cu(001) in hydrochloric acid which reveals that the presence of water and cations in the outer double layer not only introduces relaxations in the spacing of the chemisorbed chloride and the first metal layers but also a reversal of a subsurface lattice modulation as compared to that observed in UHV. For better understanding of the structural differences in UHV and in electrochemical environment, we estimate the difference of the work function introduced by the electrolyte and discuss its influence on the structure of the adsorbate complex.¹⁰

Halide adlayers in electrochemical environment¹ as well as the corresponding halogen adlayers formed in the gas phase¹¹ adsorb on the (001) surface of most fcc metals in form of a simple low-order commensurate $c(2 \times 2)$ structure with $P4mm$ symmetry, where the adsorbates reside in the energetically strongly preferred fourfold-hollow sites of the metal substrate lattice.^{12–15} A prototypical system for halide adsorption on fcc(001) surfaces and for which the adsorption process has been studied by SXR and by electrochemical methods is Br on Ag(001).^{10,16,17} For increasing potential a second-order phase transition from a lattice gas to an ordered $c(2 \times 2)$ structure has been found for the bromine adlayer. Also the adsorption of Cl on Cu(001) is an important, well-studied example of this $c(2 \times 2)$ adlayer. It has been reported for chlorine adlayers under UHV conditions^{18–25} as well as in chloride-containing electrolytes.^{6,7,26–31} However, at the electrochemical interface the $c(2 \times 2)$ structure was observed only positive of a critical potential ($-0.4 \text{ V}_{\text{Ag}/\text{AgCl}}$ at a Cl concentration of 10^{-3} M) by *in situ* STM, whereas at more negative potentials the (1×1) substrate lattice was visible, suggesting a potential-induced order-disorder phase transition into a dilute adlayer of highly mobile chloride.^{28,30} More

recently, the surface-normal interface structure of the $c(2 \times 2)$ adlayers of Cl and Br on Cu(001) was studied by *in situ* SXRD, focusing on the halide-copper interlayer spacing.^{6,7} Specifically, the dependence of the Br adlayer spacing on potential was found to be stronger than that of the Cl adlayer, which was attributed to a more ionic character of the Cl and an almost discharged Br adsorbate, respectively. Similar SXRD measurements of Cl on Cu(001) surfaces under UHV conditions by Tolentino *et al.*¹⁸ as well as earlier angle-resolved photoemission studies by Wang *et al.*³² indicated that the $c(2 \times 2)$ superstructure extends to the second atomic copper layer in form of a small subsurface buckling, an effect that was also reported for the $c(2 \times 2)$ Br adlayer in the *in situ* SXRD study by Saracino *et al.*^{6,7}

In this work we present detailed *in situ* SXRD and complementary DFT results on the adsorption behavior and interface structure of Cu(001) electrodes in chloride-containing electrolyte, focusing on the buckling in the second Cu layer. These studies allow to directly compare the Cu surface structure in the presence of the $c(2 \times 2)$ Cl adlayer and after disordering and partial desorption of the Cl with corresponding data for Cl-covered and clean Cu(001) surfaces under UHV conditions, respectively. In particular, the influence of the electrochemical environment on the copper subsurface buckling will be discussed. As reference for the surface structure of the $c(2 \times 2)$ Cl adlayer at the Cu(001)-vacuum interface we will use the recent SXRD study by Tolentino *et al.*¹⁸ SXRD provides direct, highly accurate structural data that can be modeled on the basis of simple kinematic diffraction theory. Results by this technique therefore seem more reliable than those obtained by electron diffraction methods, where more complex modeling by dynamic scattering theory is required.

II. EXPERIMENTAL

A. Surface x-ray diffraction

The x-ray scattering experiments were performed at the ID 32 beamline of the European Synchrotron Radiation Facility in Grenoble using a photon energy of 22.5 keV and a grazing incidence angle of 0.44°. The Cu(001) single-crystal sample (Mateck, 99.999%, 4 mm diameter, miscut <0.1°) was prepared prior to the experiments by electropolishing in 70% orthophosphoric acid. Subsequently, the sample was covered by a droplet of milli-Q water and mounted into the electrochemical hanging meniscus cell described in Ref. 33. In all experiments 10 mM HCl solution prepared from suprapur hydrochloric acid (Merck) and milli-Q water was used as electrolyte. All potentials were measured versus a Ag/AgCl (3 M KCl) reference electrode. During the measurements the liquid meniscus in contact with the surface was kept under high-purity nitrogen (air liquid, 99.999%) to remove dissolved oxygen from the electrolyte.

In the crystal truncation rod (CTR) studies the integrated intensities $|F_{\text{hkl}}|^2$ (where F_{hkl} is the structure factor) of different reflections (hkl) were measured in z axis geometry by rotating the sample about its surface normal. The background-subtracted integrated intensities were corrected for the Lorentz factor, polarization factor, active sample area,

and the rod interception appropriate for the z axis geometry.³⁴ Since the specular rod was recorded in $(\theta-2\theta)$ geometry, for which different corrections for the active sample area and the rod interception have to be applied than for the nonspecular CTRs, its intensity distribution had to be corrected by an additional scaling factor. Errors due to photon statistics and systematic errors in data acquisition are taken into account. The latter was estimated from deviation of measured integrated intensities of symmetry equivalent reflections to 20% and is the dominating contribution. The structure was determined by a fit of the simulated square of the structure factors to the experimental ones and a χ^2 minimization using the code “fit” (Ref. 35) which allows a three dimensional structural refinement of the SXRD data.^{36–38} The parameter error Δx of the best fit value x is determined by $\chi^2(x+\Delta x) = \chi^2(x) + 1$.

Standard bulk coordinates of the Cu(0 0 1) surface ($a_1 = a_2 = a_3 = 3.615 \text{ \AA}$, $\alpha = \beta = \gamma = 90^\circ$) are used in the following. The momentum-transfer vector is then defined by $Q = Hb_1 + Kb_2 + Lb_3$ with $a_i b_j = 2\pi \delta_{ij}$ where H, K, L , are the diffraction indices. The index L is along the direction perpendicular to the surface. The indices of the crystal truncation rods are given by $(H+K=2n)$ and the ones for rods from the reconstructed surface are determined by $(H+K=2n+1)$.

B. Density functional theory

The density functional theory (DFT) calculations were performed using the Vienna *ab initio* simulation program (VASP) developed at the Institut für Materialphysik of the Universität Wien.^{39–42} The generalized gradient approximation by Perdew and Wang (PW91-GGA) (Ref. 43) is applied to the exchange-correlation energy-functional. All atoms except Ca are described by projector augmented wave (PAW) pseudopotentials as introduced by Blöchl *et al.*⁴⁴ Ca atoms are described by ultrasoft pseudopotentials. The potentials for VASP from the database are used.⁴⁵

The Cu(001) surface is simulated by a slab geometry with a supercell containing 15 Cu layers and a $p(2 \times 2)$ surface unit cell. The theoretical lattice constant for Cu of $c = 3.636 \text{ \AA}$ is assumed, which is slightly larger than the experimental lattice constant $c = 3.615 \text{ \AA}$. The Cl atoms are adsorbed on both sides of the slab forming a $c(2 \times 2)$ superstructure, with the Cl atoms occupying hollow positions of the Cu(001) surface. The kinetic-energy cutoff of the plane-wave basis set has been chosen equal to 280 eV, and the integrals over the Brillouin zone are approximated by sums over special \mathbf{k} points. We use a 6×6 Monkhorst-Pack set of equidistant \mathbf{k} points⁴⁶ parallel to the surface. Atomic positions were relaxed until the residual forces acting on the Cu and Cl atoms are less than 1 meV/Å. The maximum allowed residual force has been chosen rather small because the atomic displacements of interest in this work are only of the order of few mÅ. In this way, the surface structure under UHV conditions can be calculated.

The Cu(001)- $c(2 \times 2)$ Cl surface becomes much more difficult to describe when in contact with an electrolyte. Different approaches to simulate electrochemical interfaces have been developed and are described in the literature.^{7,47–52} Here

we follow two different simple approaches in order to obtain a qualitative impression of the effects on the Cu surface relaxation induced by the presence of the electrolyte: (i) a homogeneous electric field of the order of $0.3\text{--}0.9\text{ V/\AA}$ is applied perpendicular to the slab⁵³ to simulate the electric field in the Helmholtz layer. In the bulk the electric field is screened by the induced surface charge density. The electrostatic potential has a discontinuity in the middle of the vacuum region. In this way the perturbing potential can be taken to be periodic. We monitor the additional displacement of the Cl and the Cu atoms induced by the electric field together with its induced screening charge density. (ii) Following the method described (and already applied to Cu(001)/halogen/electrolyte interfaces) by Saracino *et al.*,⁷ two Ca atoms are placed in the middle of the vacuum region within each supercell. They are located atop the two Cl atoms in the $p(2\times 2)$ surface unit cell, but in view of the large separation between the Ca and the surface atoms we expect displacement of the Ca atoms parallel to the surface to be of only minor importance for the effects investigated here. Electrons are transferred from the Ca atomic layer to the metal-halogen slab. This charge transfer results in an electric field in front of the metal. Furthermore, two pairs of water molecules, located on top of each other, have been added to each side of the slab. As in Ref. 7, the H-atoms point toward the surface, and the O atoms lie above the Cl atoms. During the subsequent relaxation, the Cl atoms and the Cu atoms in the outermost six layers of the slab as well as the H and O atoms of the water molecule are allowed to move, with each O-atom being restricted to an axis perpendicular to the surface. The residual forces acting on the water molecules are less than 3 meV/\AA . In order to control the pressure exerted on the surface, calculations have been carried through for different thickness of the region between the slabs.

III. RESULTS

A. Surface x-ray diffraction

In the initial phase of the experiments the Cu(001) surface was characterized by cyclic voltammetry, recorded in the SXRD cell, and parallel measurements of the scattered x-ray intensity at selected positions along the substrate's CTRs and $c(2\times 2)$ superstructure rods (Fig. 1). Specifically, the potential-dependent intensity at $(1, 0, 0.1)$ and $(1, 1, 0.1)$, i.e., the $c(2\times 2)$ superstructure rod and the anti-Bragg position of the lowest-order Cu(001) CTR, was monitored. The intensity measured at $(1, 0, 0.1)$ is proportional to the square of the coverage of the Cl induced $c(2\times 2)$ superstructure, whereas data monitored at the anti-Bragg position $(1, 1, 0.1)$ is sensitive to the coverage of all Cu-hollow sites occupied with Cl atoms, independent of the degree of order.¹⁷ Recording the potential dependent intensity of both the superstructure rod and the anti-Bragg position is therefore indispensable to determine independently the coverages for both adlayer phases, the two-dimensional lattice gas as well as the Cl $c(2\times 2)$ superstructure. In the voltammogram, Cl adsorption and desorption manifests in form of broad peaks between $\approx -0.35\text{ V}$ and the onset of hydrogen evolution near -0.70 V (the additional cathodic current in this potential

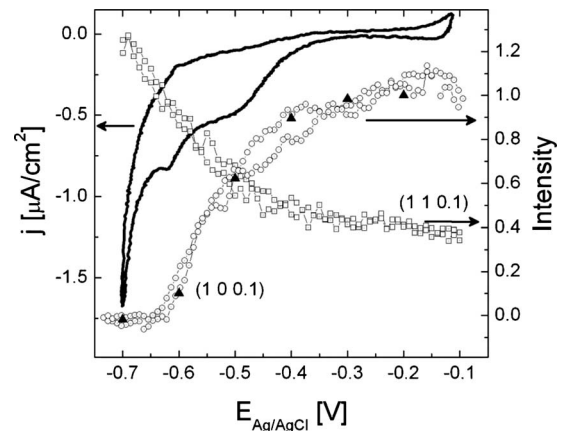


FIG. 1. Cyclic voltammogram (scan rate 10mV/s) of Cu(001) in 10 mM HCl (solid line) as well as potential-dependent intensity of the Cl superstructure rod at $(1, 0, 0.1)$ and the Cu CTR at $(1, 1, 0.1)$. In addition, the intensities measured after a step from -0.2 V to different potentials are indicated (filled triangles).

range may be related to the reduction of small amounts of residual oxygen in the cell). During the chloride adsorption process the intensity at the anti-Bragg position decreases while the intensity at the superstructure rod increases from zero at the negative potential limit to a saturation value at potentials positive of $\approx -0.35\text{ V}$. Potential-step experiments show that the intensity change occurs on time scales shorter than the time resolution of the SXRD experiments (0.5 s) and is highly reversible (as also seen in the potential-sweep experiment in Fig. 1). Such a behavior can only be attributed to the desorption and disordering of the chloride adlayer, whereas other structural changes such as potential-induced variations in the surface roughness can be excluded. Furthermore, no evidence of other ordered Cl adlayer structures was found in in-plane scans along high-symmetry directions. The latter as well as the absence of potential-induced surface roughening is in excellent agreement with the extensive previous *in situ* STM studies of this system.

According to these measurements, residual $c(2\times 2)$ ordering exists down to potentials close to the onset of hydrogen evolution and only completely disappears at -0.62 V . This $c(2\times 2) \leftrightarrow (1\times 1)$ transition manifests in form of small peaks in the cyclic voltammogram and occurs at substantially more negative potentials than those where the $c(2\times 2)$ structure was observed by *in situ* STM.^{28,30} The latter most likely is caused by a high adsorbate mobility in the potential regime where the surface is only partially covered by the ordered adlayer structure, inducing rapid fluctuations in the $c(2\times 2)$ domain network on time scales beyond the temporal resolution in the earlier STM studies. Indeed, in very recent *in situ* video-STM observations positional changes of the Cl adsorbates at domain boundaries faster than 10^{-4} s were inferred.⁵⁴ The intensity curves at $(1, 0, 0.1)$ and $(1, 1, 0.1)$ are identical for potential sweeps in positive and in negative direction, indicating a highly reversible process as expected for anion adsorption. Furthermore, in potential jump experiments the same steady-state intensities were obtained after the potential step (Fig. 1, filled triangles), typically faster than the experimental time resolution (1 s). Consequently,

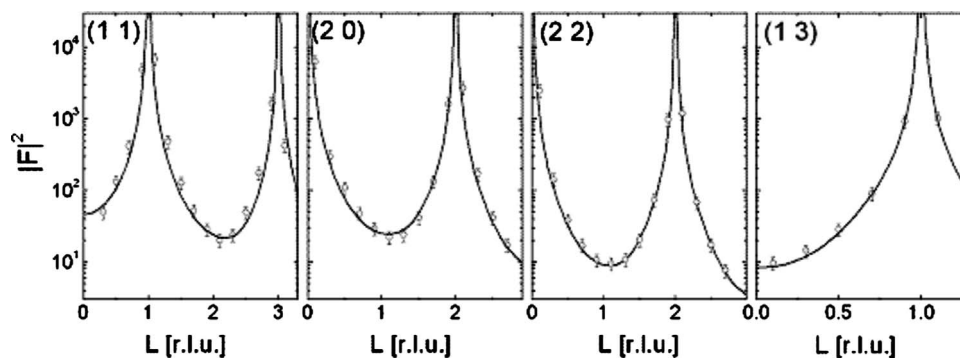


FIG. 2. Experimental crystal truncation rods of Cu(001) in 10 mM HCl at -0.70 V (circles) and best fit based on a relaxed bulk like structure (lines).

the curves in Fig. 1 represent the potential-dependent equilibrium state of this adsorbate system.

These results are at variance with recent SXRD experiments on Cu(001) in Br-containing solution by Saracino *et al.*⁷ In that study the intensity at $(1, 0, 0.1)$ on the superstructure rod was found to be nearly constant over the entire double layer potential range, even at negative potentials, where the corresponding voltammogram exhibited similar Br adsorption and desorption peaks as visible in Fig. 1. The reason for this discrepancy, not only to our SXRD results but also to the electrochemical and previous *in situ* STM data,²⁸ is currently unclear. However, the behavior observed in this study is almost identical to that found by *in situ* SXRD for bromide and chloride adsorption on Ag(001) electrodes, where likewise a continuous order-disorder transition to a $c(2 \times 2)$ phase with very similar x-ray intensity curves was reported.^{10,16,17} Specifically, for Br on Ag(001) the intensity at $(1, 1, 0.1)$ was found to increase toward more negative potentials, as in the system studied here, reaching a saturation value only 300 mV negative of the potential where the $c(2 \times 2)$ superstructure peak disappeared. This behavior was attributed to the presence of a disordered 2D lattice gas of adsorbates which partly occupy fourfold hollow and partly other adsorption sites. Also for Cl on Cu(001) an analogous lattice gas most likely exists negative of the phase transition potential, although the complete desorption of the anion adlayer apparently only occurs deep within the hydrogen evolution regime and hence was not accessible in the SXRD experiments. The chloride desorption process on Cu(001) with a remaining $c(2 \times 2)$ structure is stretched over a range of 300 mV, whereas the Br desorption process on Ag(001) with a remaining $c(2 \times 2)$ structure only takes place over a potential range of 200 mV. This indicates that the desorption process is slower for Cl on Cu(001) than for Br on Ag(001) which can be explained by the less noble character of the copper substrate compared to silver and the higher ionicity of the chloride compared to bromide inducing a stronger binding with larger attractive interaction between the substrate and adsorbate.

Detailed studies of the interface structure were performed at -0.20 V, where the surface is fully covered by the $c(2 \times 2)$ Cl superstructure (Fig. 2), and at -0.70 V, i.e., ≈ 100 mV negative of the order-disorder phase transition potential (Fig. 3). At both potentials we measured the $(1, 1,$

$L)$, $(2, 0, L)$, $(2, 2, L)$ and $(1, 3, L)$ CTRs and obtained a set of 48 nonequivalent reflections. At -0.20 V in addition the specular rod and the $(1, 0, L)$ and $(1, 2, L)$ superstructure rods were recorded, with in total 44 integrated intensities $|F_{hkl}|^2$ at nonequivalent reciprocal space positions (hkl) . The L dependent diffuse background of the $(1, 0, L)$ superstructure rod was determined carefully and subtracted. Due to the errors associated with this procedure, the errors of the integrated intensities of the $(1, 0, L)$ rod increase at lower L . The integrated intensities of the rods recorded at the two different potentials were taken in the same geometry on the same sample. The CTR data at both potentials is fully consistent with the potential dependence of the x-ray intensity shown in Fig. 1.

The CTRs obtained at -0.70 V were fitted to a structural model assuming a Cu(001)- (1×1) surface and a relaxation of the layer spacing d_{12} between the copper surface layer and the underlying bulk lattice (for all following Cu layers the Cu bulk spacing was used). In addition, the anisotropic Debye-Waller factors for the first two Cu layers, an isotropic Debye-Waller factor for the third layer and an overall scale factor were optimized in the fit. In analogy to the Br/Ag(001) adsorbate system^{10,16} a partial occupation of the fourfold-hollow sites with Cl adsorbates was assumed to model the disordered 2D lattice gas of chloride. Models without this disordered Cl adlayer also provided good fits of the experimental data and resulted in very similar vertical relaxations, but led to unusually small Debye-Waller factors of the Cu surface layer. The parameters for the best fit ($\chi^2=2.37$), which describes well the measured CTRs (Fig. 2, solid lines), are shown in Table I, together with the parameters obtained in SXRD measurements by Mironets *et al.* for a bare Cu(001) surface in UHV.⁵⁵ The Cl coverage 80 mV negative of the order-disorder transition is 0.15 ML which is in good agreement with the values found for Br on Ag(001) (Refs. 10 and 16) at corresponding potentials, i.e., 55 mV negative of the order-disorder transition taking into account the broader desorption regime of the chloride. However, this observation differs strongly from the zero coverage reported by Huemann *et al.* for the same system at the negative end of the double layer regime.⁶ In the latter study a decrease rather than an increase in the intensity at $(2, 0, L)$ was found toward negative potentials, contrary to our experimental data. This is probably the main cause of the different results in that study.

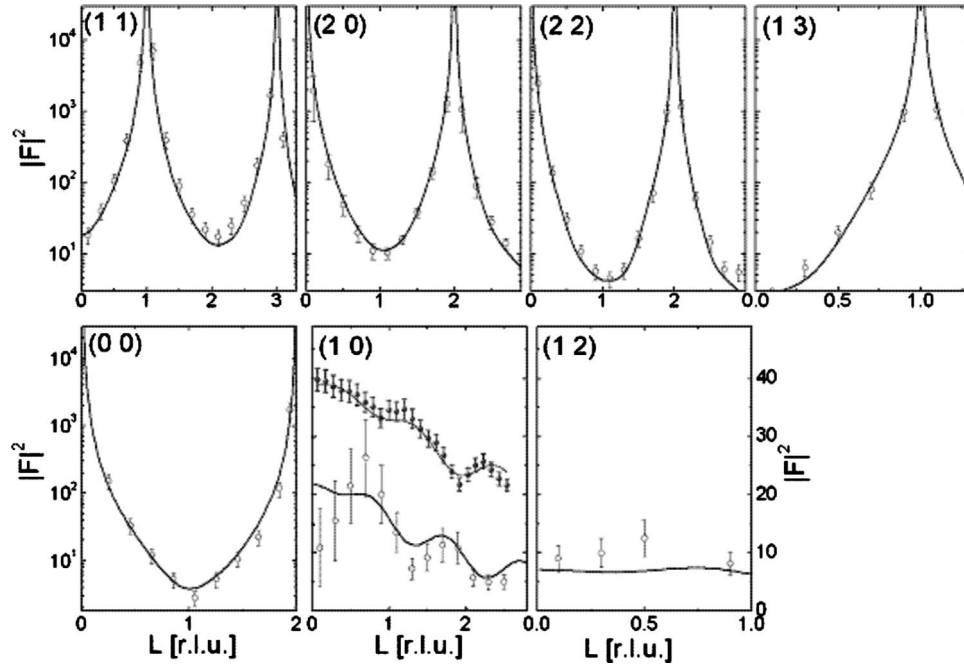


FIG. 3. Experimental crystal truncation rods and the lowest-order $c(2 \times 2)$ superstructure rod for Cu(001) in 10 mM HCl at -0.20 V (circles), together with the best fit based on the structural model described in the text (lines). Shown in the figures are also the measured $(1, 0, L)$ superstructure rod of the $c(2 \times 2)$ Cl structure in UHV (from Ref. 18, filled symbols), which is antiphase shifted relative to the data obtained in electrochemical environment.

Unfortunately, only the $(2, 0, L)$ CTR was measured at the negative limit, prohibiting a more detailed comparison. For the first layer a slight inward relaxation of 1.0% is found in our analysis, which directly manifests in the experimental data as a shift of the CTRs minima toward higher L . Within the experimental errors this relaxation is identical to that obtained for clean copper in UHV.⁵⁵

Fits of the data measured at -0.20 V employed a model of a $c(2 \times 2)$ Cl adlayer as confirmed by STM measurements in chloride containing electrolytes^{6,25–28} and supported by in-plane scans along high-symmetry directions of the Cu(001) surface. The spacing between the Cl adlayer and the Cu surface layer d_{Cl} as well as the topmost two layer spacings in

TABLE I. Fit parameters for Cu(001)- (1×1) in 10 mM HCl at -0.70 V (this work) and under UHV conditions at 160 K (from Ref. 55). The values were given in Ref. 55 as rms vibrational amplitudes in Å and converted to Debye-Waller factors via $\langle u_s^2 \rangle = B_j / (16\pi^2)$.

	(1×1) at -0.70 V	(1×1) in UHV (Ref. 55)
$d_{Cl}(\text{Å})$	1.782 ± 0.030	
$d_{12}(\text{Å})$	1.785 ± 0.020	1.777 ± 0.028
$d_{23}(\text{Å})$	1.808 ± 0.020	1.806 ± 0.026
$d_{34}(\text{Å})$	1.808 ± 0.020	1.809 ± 0.026
$d_{45}(\text{Å})$	1.808 ± 0.020	1.807 ± 0.018
DW(Cl)	2.8 ± 0.1	
DW(Cu ₁)	1.75 ± 0.05	1.876 ± 0.036
DW(Cu _{1⊥})	1.18 ± 0.11	2.052 ± 0.098
DW(Cu ₂)	0.74 ± 0.08	1.087 ± 0.010

the Cu substrate d_{12} and d_{23} were allowed to relax (see also Fig. 4). Furthermore due to the presence of distinct intensity oscillations in the $(1, 0, L)$ superstructure rod (see Fig. 3) we allow in the second Cu layer different vertical positions for atoms directly below the Cl adsorbate atoms and the Cu atoms in between those. This small subsurface buckling of amplitude Δ_2 will be the focus of the following section. Qualitatively speaking, the intensity oscillations in the $(1, 0, L)$ rod are caused by the interference of waves scattered at atomic layers, which are parallel to the surface plane and have a defined vertical distance as well as a phase difference between each other. The lateral periodicity within these layers has to be identical to that of the superstructure, with the Cl adsorbates on top of the Cu(001) forming the upper layer. The second layer has to result from a subsurface modulation with the same $c(2 \times 2)$ symmetry. It can be unambiguously identified as the buckling of the second layer, as the period of the oscillations of the superstructure rod is approximately one reciprocal lattice unit (see Fig. 3), corresponding to a vertical distance of 3.615 Å. This model is additionally sup-

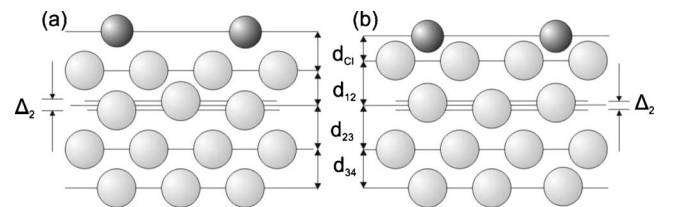


FIG. 4. Side view of the structural model for the $c(2 \times 2)$ Cl adlayer on Cu(001) in (a) electrochemical environment and (b) at the metal-vacuum interface, illustrating schematically the lattice relaxation and the buckling of the second Cu layer.

TABLE II. Fit parameters for $c(2 \times 2)$ Cl-covered Cu(001) in 10 mM HCl at -0.20 V (this work) and under UHV conditions (Ref. 18).

	$c(2 \times 2)$ at -0.20 V	$c(2 \times 2)$ in UHV (Ref. 18)
$d_{\text{Cl}}(\text{Å})$	1.856 ± 0.015	1.585 ± 0.006
$d_{12}(\text{Å})$	1.794 ± 0.015	1.839 ± 0.005
$d_{23}(\text{Å})$	1.822 ± 0.025	1.825 ± 0.003
$\Delta_2(\text{Å})$	$+0.025 \pm 0.0070$	-0.012 ± 0.003
DW(Cl)	2.39 ± 0.17	2.61
DW(Cl _⊥)	2.05 ± 0.19	0.44
DW(Cu)	1.64 ± 0.03	1.39
DW(Cu _{1⊥})	0.35 ± 0.06	
DW(Cu ₂)	0.70 ± 0.03	0.7

ported by symmetry arguments: the $c(2 \times 2)$ superstructure exhibits $p4mm$ symmetry with two perpendicular mirror planes crossing at the free hollow site of the Cu(001) bulk unit cell and a fourfold rotation axis also located at the free hollow site. All atoms of the unit cell are located at high-symmetry positions and therefore lateral displacements are forbidden by the symmetry. In addition all copper atoms of the first (or in fact any odd) Cu layer are equivalent and therefore a buckling in those layers is forbidden. Additional free fit parameters were anisotropic Debye-Waller factors for the first two Cu layers, an isotropic Debye-Waller factor for the third Cu layer, and the overall scale factor. The latter was found to be within 2% of the scale factor determined by the fit of the data at -0.70 V, indicating a consistent fit of the two surface structures. Table II summarized the parameters of the best fit ($\chi^2=2.85$) together with those obtained by Tolentino *et al.* for this adsorbate system under UHV conditions;¹⁸ the corresponding calculated CTRs and superstructure rods are included in Fig. 3 (solid lines) and obviously provide a good quantitative description of the experimental data. The structural parameters of the $c(2 \times 2)$ Cl superstructure in the two environments strongly differ, as will be discussed in more detail in the following sections. Specifically, the second-layer Cu atoms located directly below the Cl adsorbates are at lower vertical positions than the atoms in between the adsorbed Cl, opposite to the observations at the metal-vacuum interface.¹⁸

The presence and qualitative behavior of this subsurface buckling can be directly seen in the experimental data. As shown in Fig. 3, the $(1, 0, L)$ superstructure rods measured in vacuum and electrochemical environment exhibit a clear difference, namely, a phase shift of the oscillations relative to each other by 0.5 reciprocal lattice units. In the following we will show that this phase shift is the direct result of a reversal in the second Cu layer buckling at the electrochemical interface as compared to that found in UHV. The intensity of the superstructure rod is due only to scattering from atoms obeying the symmetry of the superstructure, i.e., the adsorbate layer and the second copper layer within our model. Placing these atoms at $\vec{r}_{\text{Cu } a} = \begin{pmatrix} 0 \\ \Delta_2/2 \end{pmatrix}$, $\vec{r}_{\text{Cu } b} = \begin{pmatrix} a/\sqrt{2} \\ -\Delta_2/2 \end{pmatrix}$ and $\vec{r}_{\text{Cl}} = \begin{pmatrix} 0 \\ d \end{pmatrix}$, where $d = d_{\text{Cl}} + d_{12}$ is the vertical distance of the chloride adlayer to the average vertical positions of the second-layer Cu

atoms and the buckling amplitude Δ_2 is positive if the copper atom beneath the chloride atom is lifted, the intensity distribution along the $(1, 0, L)$ rod is given by

$$I \propto |f_{\text{Cl}} e^{i q_z d} + f_{\text{Cu}} (e^{i q_z \Delta_2/2} + e^{i \pi} e^{-i q_z \Delta_2/2})|^2 \\ \approx f_{\text{Cl}}^2 + f_{\text{Cu}}^2 (q_z \Delta_2)^2 + 2 f_{\text{Cl}} f_{\text{Cu}} q_z \Delta_2 \sin(q_z d). \quad (1)$$

Here the Debye-Waller factor is included in the structure factors for chloride (f_{Cl}) and copper (f_{Cu}) and Δ_2 is assumed to be much smaller than d . The oscillations of the intensity of the superstructure rod are represented by the third summand in Eq. (1), which includes the term $\sin(d q_z)$. This simple calculation in kinematical approximation shows clearly that exclusively the buckling amplitude Δ_2 and the vertical distance d between the second Cu layer and the Cl adlayer affect the amplitude and the period, respectively, of the intensity oscillation of the superstructure rod. This implies especially that a significant correlation between the parameter pair (Δ_2, d) and the remaining structural parameters can be excluded. For that reason, this small effect can be unambiguously detected, although the buckling amplitude is similar to the errors in the interlayer spacings. The above consideration also confirms the assumed model: the extension of the superstructure to another Cu layer than the second would affect the oscillation period and an additional layer would result in additional oscillations with different period. Reversal of the buckling, i.e., inversion of the sign of Δ_2 , causes an antiphase shift in the oscillations. Hence, the two central qualitative observations for the $(1, 0, L)$ rod—the extension of the $c(2 \times 2)$ to the second Cu layer and the different sign of the buckling in UHV and electrochemical environment—can already be deduced from this simplified analysis. In addition, the CTR analysis indicates a 17% expansion of the Cl-Cu interlayer spacing as compared to that found in UHV,¹⁸ in agreement with the *in situ* SXRD results by Huemann *et al.*⁶

B. Calculation of second-layer Cu-atom buckling

In this section we argue that the reversal of the sign of the corrugation of the second-layer Cu atoms at the electrochemical interface, as opposed to UHV, can be reproduced by density functional calculations. DFT calculations for this system have been carried through by Saracino *et al.*,⁷ who mentions a small buckling to result from their calculations. Here we focus on this subsurface buckling, which was not quantified explicitly in the previous DFT work. In order to relate to literature we will also quote our calculated Cl-Cu and Cu-Cu interlayer separations. Initial calculations for the clean Cl-free Cu(001) surface yield an interlayer separation of the two topmost Cu layers of 1.76 Å, which corresponds to a 3% contraction with respect to the bulk value. This agrees within the error bars with previous theoretical (GGA or LDA) results,^{14,56} and it is consistent with the experimental SXRD results for a clean Cu(001) surface under UHV conditions⁵⁵ and in 10 mM HCl at -0.70 V (see Table I). For the $c(2 \times 2)$ Cl covered Cu(001) surface in the absence of external electric fields or additional species, i.e., the surface under UHV conditions, we obtain a Cl-Cu interlayer separation $d_{\text{Cl}} = 1.667 \pm 0.012$ Å in agreement with Ref. 7 and an average spacing between the two topmost Cu layers d_{12}

TABLE III. Calculated surface atomic geometry of $c(2 \times 2)$ Cl-covered Cu(001) in the presence of external applied electric fields, additional water molecules, and water and Ca counter ions. For the latter case also the height L_z of the supercell is given. Vac denotes a vacuum layer. The estimated error of the second Cu layer corrugation is 0.004 \AA .

	L_z (\AA)	d_{Cl} (\AA)	d_{12} (\AA)	Δ_2 (\AA)
$c(2 \times 2)$ -Cl at 0 V/ \AA	Vac	1.67	1.82	-0.006
$c(2 \times 2)$ -Cl at 0.3 V/ \AA	Vac	1.68	1.82	-0.005
$c(2 \times 2)$ -Cl at 0.9 V/ \AA	Vac	1.71	1.82	-0.004
$c(2 \times 2)$ -Cl+H ₂ O	44.27	1.70	1.80	-0.002
$c(2 \times 2)$ -Cl+H ₂ O+Ca	44.27	1.79	1.77	+0.006
$c(2 \times 2)$ -Cl+H ₂ O+Ca	45.27	1.81	1.79	+0.0034
$c(2 \times 2)$ -Cl+H ₂ O+Ca	46.27	1.82	1.81	+0.0026

$= 1.817 \pm 0.01 \text{ \AA}$. Saracino *et al.* have reported a first Cu-Cu layer spacing 0.6% larger than the bulk value,⁷ which is within the error bar of our calculation. The 3% contraction of the interlayer separation between the topmost two Cu layers of the clean Cu(001) surface vanishes upon Cl adsorption, which is ascribed to the charge transfer from the Cu surface to the negatively charged Cl ions.⁵⁷ The buckling amplitude of the second Cu layer is $\Delta_2 = -0.006 \text{ \AA}$, with a convergence error of about $\pm 0.004 \text{ \AA}$ estimated from additional calculations with different number of Cu layers, vacuum thickness, k -point sets, and cutoff energy. This value is compatible with the experimental corrugation under UHV conditions found in the SXRD measurements by Tolentino *et al.*,¹⁸ taking the errors in the experimental and DFT studies into account.

In a first approach, the effect of the outer part of the electrochemical double layer on the Cu surface relaxation was simulated by applying a homogeneous electric field to the $c(2 \times 2)$ Cl slab. The electric field vector is parallel to the surface normal and points toward the Cu surface. This corresponds to an induced negative screening charge at that surface. In response to the applied electric field the corrugation of the second-layer Cu atoms decreases, as can be seen in Table III. However, the applied fields in the range of $0.3 \text{ V/\AA} - 0.9 \text{ V/\AA}$ are not sufficiently strong to reverse the buckling. The average interlayer separation between the two first metal layers d_{12} decreases only insignificantly as the electric field is switched on, while the Cl-Cu separation increases in agreement with the trend reported in Ref. 7. The qualitative trends are thus the same as derived from the comparison of the present SXRD experiments with the data by Tolentino *et al.*¹⁸ but the effect is too small, at least for the electric field strengths considered here.

In all following DFT calculations the electrochemical interface was modeled by additionally introducing species of the outer Helmholtz layer—specifically water and counter ions—into the supercell, whose height was chosen equal to 44.27 \AA . If solely water molecules are added to the system the corrugation decreases to $\Delta_2 = -0.002 \text{ \AA}$ while the Cl-Cu interlayer separation increases (in comparison to the surface in UHV) to $d_{\text{Cl}} = 1.70 \text{ \AA}$ and the topmost Cu interlayer separation contracts to $d_{12} = 1.80 \text{ \AA}$. This trend fits to the concep-

tion that the Cl ion is partially screened by the water dipoles, thereby weakening the Cl-Cu bond and strengthening the attractive interaction between the two topmost Cu layers.⁵⁰

Finally, we have added both the water molecules and Ca atoms into the vacuum region between the slabs. For this system occurs a charge transfer from the Ca atoms to the slab, which results in an electric field in the electrolyte region. Upon structural optimization of the $c(2 \times 2)$ Cl surface as described above (see Sec. II B), the relaxation pattern changes distinctly more pronounced than in the calculations where the electric field was directly applied. The results are summarized in Table III for different size L_z of the supercell in the direction perpendicular to the surface. We note that the total energy adopts a minimum between $L_z = 45$ and 46 \AA , corresponding to the condition of zero pressure. Additional calculations at different L_z but frozen position of the top layer Cu and Cl atomic positions corroborate the interpretation that a significant part of the variation in Δ_2 in Table III is related to the different amount of charge transfer as a function of L_z . The largest effect on the Cu corrugation Δ_2 can be observed for $L_z = 44.27 \text{ \AA}$ (for which, however, the pressure does not vanish). In this case, the Cl-Cu interlayer separation further increases to $d_{\text{Cl}} = 1.79 \text{ \AA}$ whereas the average spacing between the first two Cu layers decreases. Most notably, the corrugation of the second-layer Cu atoms reverses its sign as compared to the surface under UHV conditions and becomes $\Delta_2 = 0.006 \text{ \AA}$. Hence, our DFT calculations reproduce the intriguing effect of the electrolyte on the subsurface buckling of the second Cu layer. To relate this result for $L_z = 44.27 \text{ \AA}$ to the relaxations caused by an electric field (Table III, top 3 rows) we note that the screening charge density at the Cu surface atoms is roughly a factor of four larger than in case of the $0.9[\text{V/\AA}]$ electric field. The larger effect may therefore be a consequence of the larger induced charge density.

IV. DISCUSSION

As already discussed in the previous studies by Huemann *et al.*⁶ and Saracino *et al.*,⁷ the interface structures of the $c(2 \times 2)$ Cl adlayer on Cu(001) in electrochemical environment and at the metal-vacuum interface exhibit notable differences, which can be attributed to the presence of the outer Helmholtz layer. They are schematically indicated in the structural models shown in Figs. 4(a) and 4(b). In agreement with the previous *in situ* SXRD results⁶ the Cu-Cl interlayer spacing of 1.856 \AA and the corresponding Cu-Cl bond length of $2.59 \pm 0.01 \text{ \AA}$ are 17% larger than that observed in UHV.¹⁸ As already pointed out by Huemann⁶ the spacing in electrochemical environment is close to that expected for ionic bonding (2.58 \AA),⁵⁸ whereas the bond-length deduced from the SXRD data in UHV is closer to the bond-length expected for a covalent bonding (2.35 \AA).⁵⁹ Furthermore, also the out-of-plane Debye-Waller factor of the chloride layers, corresponding to the chloride's vibrations perpendicular to the surface, is clearly increased at the electrochemical interface, whereas all other vibrational amplitudes are comparable in the two environments. Both effects can be attributed to a reduced binding of the Cl layer in the presence of the

electrolyte solution, caused by the solvation of the anionic adsorbates and the presence of counter ions in the diffuse layer.

Of particular interest in the present study is the small, but clearly detectable corrugation of the second copper layer. Under UHV conditions the Cu atoms below the Cl atoms are displaced toward the surface and those without Cl on top are closer to the Cu bulk [Fig. 4(b)].¹⁸ This was explained by a partial charge transfer between the copper atoms in the first copper layer and the chloride atoms, resulting in an ionic bond between the chloride and the second-layer copper atoms underneath those adsorbates. In contrast, for the $c(2 \times 2)$ structure at the electrochemical interface our *in situ* SXRD data unambiguously indicates an upward displacement of the second-layer Cu atoms situated between the Cl adsorbate positions [Fig. 4(a)], i.e., a reversal of this subsurface buckling. A buckling of the same type as in our study and with similar corrugation amplitude (0.004–0.008 Å, depending on the potential) was also found by Saracino *et al.* for the $c(2 \times 2)$ structure of bromide on Cu(001).⁷ Our DFT calculations strongly suggest that the corrugation reversal is a clear consequence of the presence of the electrolyte and apparently requires both the solvation of the Cl adsorbates by coadsorbed water as well as the electric field generated by cations in the outer Helmholtz layer. These effects modify the charge distribution in the chemisorbed adlayer and the adjacent Cu surface, which in turn may influence the structural relaxation of the top copper layers.

To better understand the relationship of $c(2 \times 2)$ Cl on Cu(001) in UHV and in electrochemical environment we estimate the potential shift introduced by the electrolyte. The potential of the metal electrode E_{Me} is given by⁶⁰

$$E_{\text{Me}} = \Phi_{\text{Me}}/e - E_{\text{ref}} + E_{\text{sol}}. \quad (2)$$

Here Φ_{Me} is the electron work function of the metal in UHV and E_{ref} is the “absolute potential” of the reference electrode. The absolute potential of the standard hydrogen electrode is approximately $E_{\text{SHE}} = 4.5$ eV,^{61,62} which corresponds to an “absolute potential” of the Ag/AgCl electrode of $E_{\text{Ag/AgCl}} = 4.7$ eV. The term E_{sol} contains potential shifts due to the contact of the electrode with electrolyte solution, which are (i) the modification of the work function when the electrode is brought in contact with the solution, (ii) the contribution of any preferentially oriented solvent molecules, and (iii) the potential drop due to the presence of free charges close to the interface. The work function of the bare Cu(001) surface is $\Phi_{001} = 4.48$ eV, however, the adsorption of Cl into a $c(2 \times 2)$ superstructure introduces a work function shift of $\Delta\Phi_{c(2 \times 2)} = +1.1$ eV.⁶³ Consequently, the difference between the Cu(001) electrode in 10 mM HCl at an applied potential of -0.2 V and the $c(2 \times 2)$ Cl in UHV corresponds to

$$E_{\text{sol}} = E_{\text{Me}} - (\phi_{001} + \Delta\phi_{c(2 \times 2)})/e + E_{\text{Ag/AgCl}} = -1.1 \text{ V}. \quad (3)$$

Hence, the Cu(001)- $c(2 \times 2)$ surface in HCl solution is substantially negatively charged as compared to the $c(2 \times 2)$ Cl structure in UHV. This charge on the electrode side is compensated by a corresponding charge formed by cations in the

outer Helmholtz layer and results in an electric field toward the Cu surface, as introduced in the calculations. Assuming the additional negative charge of the Cu(001)- $c(2 \times 2)$ in the electrochemical environment to be located on the Cl adlayer, this would correspond to a more ionic character of halide, resulting from the electrostatic screening of the chemisorbed Cl by the coadsorbed water and cations, which is supported by the consideration of the difference in bond lengths above. A higher ionicity of adsorbed halide ions under these conditions was already proposed in previous studies^{6–9} to explain the expanded halide-copper bond at electrochemical interfaces. Furthermore, Saracino *et al.* suggested a less ionic character of $c(2 \times 2)$ Br on Cu(001),⁷ which by analog reasoning as above can be attributed to the smaller work function shift [$\Delta\Phi_{c(2 \times 2)} = +0.9$ eV (Ref. 64)] induced by the Br adlayer.

Finally, we compare the structural data for the $c(2 \times 2)$ Cl-covered Cu surface at -0.20 V and the Cu(001)- (1×1) surface at -0.70 V, where the Cl adlayer is disordered. In both cases we find very similar values for the first Cu interlayer spacing, specifically an $\approx 1\%$ inward relaxation. This agrees well with the relaxation of the clean Cu(001) surface,⁵⁵ but clearly differs from that of the Cu(001)- $c(2 \times 2)$ Cl in UHV,¹⁸ which points again to pronounced changes in the nature of the adsorbate’s bond as suggested previously.^{6–9} The Cl vibration amplitudes at -0.70 V are increased in comparison to those at -0.20 V, in agreement with a disordering of the adlayer at negative potentials. The Cu-Cl spacing at -0.70 V appears smaller than that at -0.20 V, suggesting a slight change in the metal-halide bond. This is not unexpected since already under UHV conditions the adsorbate’s coverage influences its charge state. For adsorbates in electrochemical environment this effect is even stronger due to the different hydration of the adsorbates in the low coverage phases at negative potentials as compared to that in the close-packed structures at more positive potentials, where the solvent is largely displaced from the metal surface and the adlayer is partly discharged.^{1,10} However, following the arguments given previously,^{6,7} the Cl-Cu bond length should increase at more negative potentials, where the adsorbate is expected to be more ionic, or be potential independent, assuming that the Cl adsorbate on Cu(001) is largely ionic even in the $c(2 \times 2)$ phase.^{6,7} A similar effect was observed for Cl adsorption on Au(111), where the existence of a weaker bond with a longer distance at more negative potentials was revealed by x-ray absorption fine structure.⁶⁵

V. CONCLUSION

In this work we have presented detailed structural results obtained by *in situ* SXRD measurements and DFT calculations for the chloride adlayer on Cu(001) as well as discussed those data in relationship to previous studies of this and related adsorbate systems. Although Cl adsorption at the electrochemical interfaces and Cl₂ adsorption under UHV conditions result in the same $c(2 \times 2)$ superstructure, the presence of the electrolyte induces a corrugation reversal in the buckling of the second Cu layer. The subsurface struc-

tural reversal can be reproduced in the calculations by taking the outer part of the electrochemical double layer into account. The estimation of the difference in work function in electrochemical and UHV environment points toward a more negatively charged Cu(001)- $c(2 \times 2)$ surface in solution and consequently to a more ionic bonding.

In addition, potential dependent x-ray scattering measurements reveal that the $c(2 \times 2)$ structure exists down to potentials close to the onset of hydrogen evolution, where a phase transition from the $c(2 \times 2)$ structure to a disordered 2D lattice gas of chloride is observed. The disordered Cl adlayer was found to exhibit a substantial coverage even at potentials as negative as 0.7 V vs Ag/AgCl. This behavior is analogous to that of Cl and Br on Ag(001) electrodes, where a qualitatively identical continuous order-disorder transition was reported.^{10,16,17}

In general, the $c(2 \times 2)$ phases of anionic adsorbates on (001)-oriented metal surfaces represent particularly simple,

but important cases and therefore are well suited as model systems to further a true quantum theoretical understanding of electrochemical interfaces and their relationship to surfaces under UHV conditions. Detailed surface crystallographic studies as presented here as well as in a few previous publications⁶⁻⁹ provide experimental data that can be directly compared to calculations, thus allowing to test and guide the development of *ab initio* theories for the description of electrochemical phase boundaries.

ACKNOWLEDGMENTS

We thank the Deutsche Forschungsgemeinschaft for financial support via Grant No. Ma 1618/13. Calculations have been carried through at the Rechenzentrum der Universität Kiel. We acknowledge the ESRF for providing synchrotron radiation facilities and thank the ID 32 beamline staff for the technical support.

*Present address: University of Life Sciences in Lublin, Faculty of Food Science and Biotechnology, Skromna 8, 20-704 Lublin, Poland.

¹O. M. Magnussen, *Chem. Rev.* **102**, 679 (2002).

²J. K. Sass and K. Bange, in *Electrochemical Surface Science*, edited by M. P. Soriaga (American Chemical Society, Washington, 1988), Chap. 4, p. 54.

³J. K. Sass, D. Lackey, J. Schott, and B. Straehler, *Surf. Sci.* **247**, 239 (1991).

⁴J. Wang, B. M. Ocko, A. J. Davenport, and H. S. Isaacs, *Phys. Rev. B* **46**, 10321 (1992).

⁵C. A. Lucas, N. M. Markovic, and P. N. Ross, *Phys. Rev. B* **55**, 7964 (1997).

⁶S. Huemann, N. T. M. Hai, P. Broekmann, and K. Wandelt, *J. Phys. Chem. B* **110**, 24955 (2006).

⁷M. Saracino, P. Broekmann, K. Gentz, M. Becker, H. Keller, F. Janetzko, T. Bredow, K. Wandelt, and H. Dosch, *Phys. Rev. B* **79**, 115448 (2009).

⁸O. Endo, M. Kiguchia, T. Yokoyama, M. Ito, and T. Ohta, *J. Electroanal. Chem.* **473**, 19 (1999).

⁹O. Endo, H. Kondoh, Y. Yonamoto, T. Yokoyama, and T. Ohta, *Surf. Sci.* **463**, 135 (2000).

¹⁰Th. Wandlowski, J. X. Wang, and B. M. Ocko, *J. Electroanal. Chem.* **500**, 418 (2001).

¹¹P. A. Dowben, *CRC Crit. Rev. Solid State Mater. Sci.* **13**, 191 (1987).

¹²T. Kramar, D. Vogtenhuber, R. Podlucky, and A. Neckel, *Electrochim. Acta* **40**, 43 (1995).

¹³A. Ignaczak and J. A. N. F. Gomes, *J. Electroanal. Chem.* **420**, 71 (1997).

¹⁴A. Migani, C. Sousa, and F. Illas, *Surf. Sci.* **574**, 297 (2005).

¹⁵A. Migani and F. Illas, *J. Phys. Chem. B* **110**, 11894 (2006).

¹⁶B. M. Ocko, J. X. Wang, and T. Wandlowski, *Phys. Rev. Lett.* **79**, 1511 (1997).

¹⁷J. X. Wang, T. Wandlowski, and B. M. Ocko, in *Proceedings of the Symposium on the Electrochemical Double Layer*, edited by C. Korzeniewski and B. E. Conway (The Electrochemical Society, Pennington, NJ, 1997), p. 293.

ety, Pennington, NJ, 1997), p. 293.

¹⁸H. C. N. Tolentino, M. De Santis, Y. Gauthier, and V. Langlais, *Surf. Sci.* **601**, 2962 (2007).

¹⁹D. Westphal and A. Goldmann, *Solid State Commun.* **35**, 437 (1980).

²⁰D. Westphal, A. Goldmann, F. Jona, and P. M. Marcus, *Solid State Commun.* **44**, 685 (1982).

²¹K. N. Eltsov *et al.*, *JETP Lett.* **62**, 444 (1995).

²²M. Galeotti, B. Cortigiani, M. Torrini, U. Bardi, B. Andryushchkin, A. Klimov, and K. Eltsov, *Surf. Sci.* **349**, L164 (1996).

²³M. Kiguchi, T. Yokoyama, S. Terada, M. Sakano, Y. Okamoto, T. Ohta, Y. Kitajima, and H. Kuroda, *Phys. Rev. B* **56**, 1561 (1997).

²⁴C. Y. Nakakura, V. M. Phanse, and E. I. Altman, *Surf. Sci.* **370**, L149 (1997).

²⁵C. Y. Nakakura, G. Zheng, and E. I. Altman, *Surf. Sci.* **401**, 173 (1998).

²⁶I. Villegas, C. B. Ehlers, and J. L. Stickney, *J. Electrochem. Soc.* **137**, 3143 (1990).

²⁷D. W. Suggs and A. J. Bard, *J. Phys. Chem.* **99**, 8349 (1995).

²⁸M. R. Vogt, F. A. Möller, C. M. Schilz, O. M. Magnussen, and R. J. Behm, *Surf. Sci.* **367**, L33 (1996).

²⁹T. P. Moffat, *J. Phys. Chem. B* **102**, 10020 (1998).

³⁰M. R. Vogt, A. Lachenwitzer, O. M. Magnussen, and R. J. Behm, *Surf. Sci.* **399**, 49 (1998).

³¹O. M. Magnussen, L. Zitzler, B. Gleich, M. R. Vogt, and R. J. Behm, *Electrochim. Acta* **46**, 3725 (2001).

³²L.-Q. Wang, A. E. Schach von Wittenau, Z. G. Ji, L. S. Wang, Z. Q. Huang, and D. A. Shirley, *Phys. Rev. B* **44**, 1292 (1991).

³³O. M. Magnussen, K. Krug, A. H. Ayyad, and J. Stettner, *Electrochim. Acta* **53**, 3449 (2008).

³⁴E. Vlieg, *J. Appl. Crystallogr.* **30**, 532 (1997).

³⁵<http://www.sub.uni-hamburg.de/opus/volltexte/1999/99/>

³⁶C. Kumpf, A. Müller, W. Weigand, E. Umbach, J. Wagner, V. Wagner, S. Gundel, L. Hansen, J. Geurts, J. H. Zeysing, F. Wu, and R. L. Johnson, *Phys. Rev. B* **68**, 035339 (2003).

³⁷R. Herger, P. R. Willmott, O. Bunk, C. M. Schlepütz, B. D.

- Patterson, B. Delley, V. L. Shneerson, P. F. Lyman, and D. K. Saldin, *Phys. Rev. B* **76**, 195435 (2007).
- ³⁸A. Hirnet, K. Schroeder, S. Blügel, X. Torrelles, M. Albrecht, B. Jenichen, M. Gierer, and W. Moritz, *Phys. Rev. Lett.* **88**, 226102 (2002).
- ³⁹G. Kresse and J. Hafner, *Phys. Rev. B* **47**, 558 (1993).
- ⁴⁰G. Kresse and J. Hafner, *Phys. Rev. B* **49**, 14251 (1994).
- ⁴¹G. Kresse and J. Furthmüller, *Comput. Mater. Sci.* **6**, 15 (1996).
- ⁴²G. Kresse and J. Furthmüller, *Phys. Rev. B* **54**, 11169 (1996).
- ⁴³J. P. Perdew, J. A. Chevary, S. H. Vosko, K. A. Jackson, M. R. Pederson, D. J. Singh, and C. Fiolhais, *Phys. Rev. B* **46**, 6671 (1992).
- ⁴⁴P. E. Blöchl, *Phys. Rev. B* **50**, 17953 (1994).
- ⁴⁵G. Kresse and D. Joubert, *Phys. Rev. B* **59**, 1758 (1999).
- ⁴⁶H. J. Monkhorst and J. D. Pack, *Phys. Rev. B* **13**, 5188 (1976).
- ⁴⁷A. Y. Lozovoi, A. Alavi, J. Kohanoff, and R. M. Lynden-Bell, *J. Chem. Phys.* **115**, 1661 (2001).
- ⁴⁸S. Venkatachalam, P. Kaghazchi, L. A. Kibler, D. M. Kolb, and T. Jacob, *Chem. Phys. Lett.* **455**, 47 (2008).
- ⁴⁹E. Skúlason, G. S. Karlberg, J. Rossmeisl, T. Bligaard, J. Greeley, H. Jónsson, and J. K. Nørskov, *Phys. Chem. Chem. Phys.* **9**, 3241 (2007).
- ⁵⁰J. Rossmeisl, E. Skúlason, M. E. Björketuna, V. Tripkovic, and J. K. Nørskov, *Chem. Phys. Lett.* **466**, 68 (2008).
- ⁵¹J. S. Filhol and M. Neurock, *Angew. Chem. Int. Ed.* **45**, 402 (2006).
- ⁵²C. D. Taylor, S. A. Wasileski, J. S. Filhol, and M. Neurock, *Phys. Rev. B* **73**, 165402 (2006).
- ⁵³J. Neugebauer and M. Scheffler, *Phys. Rev. B* **46**, 16067 (1992).
- ⁵⁴T. Tansel, A. Taranovskyy, and O. M. Magnussen, *Studies of Adsorbate Dynamics by In Situ Video-STM: Surface Diffusion, Adsorbate-Adsorbate Interactions, and Interactions with Defects*, 2008.
- ⁵⁵O. Mironets, H. L. Meyerheim, C. Tusche, P. Zschack, H. Hong, N. Jeutter, R. Felici, and J. Kirschner, *Phys. Rev. B* **78**, 153401 (2008).
- ⁵⁶R. Pentcheva and M. Scheffler, *Phys. Rev. B* **61**, 2211 (2000).
- ⁵⁷F. Sette, T. Hashizume, F. Comin, A. A. MacDowell, and P. H. Citrin, *Phys. Rev. Lett.* **61**, 1384 (1988).
- ⁵⁸J. C. Slater, *J. Chem. Phys.* **41**, 3199 (1964).
- ⁵⁹R. D. Shannon, *Acta Crystallogr., Sect. A: Cryst. Phys., Diffraction, Theor. Gen. Crystallogr.* **32**, 751 (1976).
- ⁶⁰S. Trasatti, *J. Electroanal. Chem.* **150**, 1 (1983).
- ⁶¹W. Schmickler, *Chem. Rev.* **96**, 3177 (1996).
- ⁶²W. Schmickler, *Interfacial Electrochemistry* (Oxford University Press, New York; Oxford, 1996).
- ⁶³D. Westphal and A. Goldmann, *Surf. Sci.* **131**, 113 (1983).
- ⁶⁴N. V. Richardson and J. K. Sass, *Surf. Sci.* **103**, 496 (1981).
- ⁶⁵O. Endo, D. Matsumura, K. Kohdate, M. Kiguchi, T. Yokoyama, and T. Ohta, *J. Electroanal. Chem.* **494**, 121 (2000).